AST325 Lab 6: Supernova Light Curves

Shimona Das
Student Number: 1008964943
Group N

March 2025

Abstract

Type Ia supernovae are standard candles that can be used to constrain the Hubble constant and measure cosmic distances. We captured the post-maximum drop of SN 2025fbf in the r-band in this lab by utilizing the T21 telescope to observe it over five nights in April 2025. A comprehensive pipeline for data reduction was put into place, which included aperture photometry, WCS-based astrometric calibration, dark subtraction, and background modeling. Using APASS DR10 standard stars to calibrate the supernova's brightness, we created a light curve from which we could estimate a peak magnitude of $m_r = 13.35 \pm 0.10$ and a decrease rate of $\Delta m_{15,r} = 1.30 \pm 0.15$. We calculated a distance modulus of $\mu = 32.86 \pm 0.14$ and an absolute magnitude of $M_r = -19.51 \pm 0.10$ using the Phillips relation. These values equate to a luminosity distance of 115^{+8}_{-7} Mpc. Despite minor systematic offsets from the redshift-derived distance, the results are consistent with a normal Type Ia supernova and demonstrate the effectiveness of small-telescope photometry in contributing to cosmological measurements.

1 Introduction

An important part of modern observational cosmology is measuring distances to astronomical objects to help characterise the expansion of the Universe. This process relies on the concept of the *distance ladder*, a succession of distance measuring techniques calibrated progressively outward into the universe. Type Ia supernovae (SNe Ia) are particularly crucial components of this ladder. These events are bright stellar explosions believed to occur when a white dwarf star, accreting mass from a companion star, surpasses the Chandrasekhar mass limit ($\sim 1.4\,M_\odot$). At this threshold, electron degeneracy pressure is no longer sufficient to stabilize the star and ultimately leads to a thermonuclear explosion dominated by carbon and oxygen fusion. The resultant explosion synthesises heavy elements and emits a bright flash of radiation.

While the physical mechanisms which underlie these explosions are actively studied, observationally Type Ia supernovae have been established as highly effective *standard candles*. Their use comes from quite a well documented empirical relationship which is known as the Phillips relation, between their peak intrinsic luminosity and the decline rate of their brightness approximately 15 days after peak. This relationship can be typically expressed as the following:

$$M_r(\mathrm{mag_{AB}}) \approx -19.6 + 0.068\,\Delta m_{15} \tag{1}$$

where M_r is the peak absolute magnitude in the r-band, and Δm_{15} is the magnitude drop observed from peak brightness to 15 days post-peak.

In this lab, the goal is to apply this relationship by measuring a newly discovered SN Ia's apparent brightness over several weeks, specifically around its peak and 15 days post-peak. By comparing the observed peak apparent magnitude (m_r) to the intrinsic absolute magnitude (M_r), the following distance modulus (μ) is observed:

$$\mu = m_r - M_r \tag{2}$$

From this distance modulus, the luminosity distance (D_L) is subsequently calculated using:

$$D_L = 10^{(\mu+5)/5}\ \mathrm{pc} \tag{3}$$

Using robotic telescopes, T21 for this lab, provided by the iTelescope network, multiple r-band images are collected over approximately three weeks to produce a light curve. Observations are planned

by selecting relatively recent (less than a week old) SN Ia candidates from the Transient Name Server (TNS) which in this case was SN2025fbf, ensuring targets are nearby (redshift $z0.05$) to maintain sufficient observational brightness. Each observational run involves short exposures totalling 15–20 minutes per night to minimise measurement errors and cost.

Standard stars from the APASS DR10 collection are used for photometric image calibration. Using reference stars, we calibrate AB magnitudes from instrumental magnitudes using aperture photometry techniques. In order to precisely ascertain the peak magnitude and the magnitude fall after 15 days, we first get the calibrated photometric measurements and then use a low-order polynomial or spline fit to match the observed data points around the peak brightness.

The last step in the study is to plot the luminosity distances against redshift in a collective Hubble diagram using the luminosity distances calculated for the entire class. Fitting this diagram allows us to extract an estimate of the Hubble constant (H_0), thereby directly measuring the current rate of cosmic expansion.

2 Data and Observation

Date	Personnel	Notes
23/03/2025	S. Das	Recorded data for SN2025dbx on T21 Utah Telescope
24/03/2025	S. Das	Recorded data for SN2025dbx on T21 Utah Telescope
25/03/2025	S. Das	Recorded data for SN2025dbx on T21 Utah Telescope
08/04/2025	S. Das	Recorded data for SN2025fbf on T21 Utah Telescope
09/04/2025	S. Das	Recorded data for SN2025fbf on T21 Utah Telescope
10/04/2025	S. Das	Recorded data for SN2025fbf on T21 Utah Telescope
15/04/2025	S. Das	Recorded data for SN2025fbf on T21 Utah Telescope

Table 1: A summary of observations

Property	**Value**
Supernova Type	Type Ia
IAU Designation	SN 2025fbf
Discoverer Internal Name	KATS25F022
Discovery Date	2025-03-19 15:42:16 UTC
Discovery Magnitude	19.18 ABMag
Discovery Filter	Clear
Redshift (z)	0.035231
Host Galaxy	UGC 3526
Host Galaxy Redshift	0.035231
Coordinates (J2000)	RA: 06:45:31.809, DEC: +53:26:59.59
Reporting Groups	XOSS, ZTF, ATLAS, YSE, Fink, GOTO
Classifying Groups	LiONS, ZTF
Telescope Used	T21 (Utah)
Imager	FLI Camera
Plate Scale	0.96 arcsec/pixel
Observed Field of View	$48.9' \times 32.6'$

Table 2: Properties of SN 2025fbf, a Type Ia Supernova observed using the T21 telescope in Utah.

3 Data Reduction

Redshift, predicted brightness, and visibility from the T21 telescope were among the favorable criteria that led us to choose SN2025dbx as our first choice. Altitude restrictions, however, hindered observations

Property	Value
Observatory	Utah Desert Remote Observatory
Telescope Designation	T21
Location (Latitude, Longitude)	37.7378° N, 113.6975° W
Altitude	1570 m
Telescope Aperture	431 mm (17 inches)
Telescope Type	Corrected Dall-Kirkham (CDK) Reflector
Mount Type	Equatorial Mount
Imager	FLI PL6303E CCD Camera
Pixel Array	3072 × 2048 pixels
Pixel Size	9 µm × 9 µm
Plate Scale	0.96 arcsec/pixel
Field of View	$48.9' \times 32.6'$
Available Filters	Luminance, Red, Green, Blue, Ha, Clear
Recommended Filter	Red (r-band)

Table 3: Specifications and properties of the T21 Telescope located at the Utah Desert Remote Observatory used for observations of SN 2025fbf.

by making it impossible to obtain useful data close to maximum light. When conditions improved, SN2025dbx was no longer suitable for accurate photometric distance estimation because it had already passed peak brightness. As a result, SN2025fbf, a novel Type-Ia candidate, was chosen. Importantly, at the time of data collection, it was still getting close to peak brightness, yet it showed comparable observational benefits.

SN2025fbf observations were made using 1×1 binning in the red filter. Every observing night, 15 exposures with a 60-second integration time were obtained. This approach was created to provide adequate temporal sampling to capture post-maximum light curve behavior while striking a compromise between the need to prevent detector saturation and signal-to-noise needs. Additionally, a set telescope allocation budget of 100 points limited the number of exposures, requiring trade-offs between statistical significance and temporal resolution. Despite being conservative, the 60-second cadence eventually offered sufficient coverage over several nights to restore the supernova's brightness progression.

All raw frames underwent preprocessing, including bias and dark adjustments. To eliminate readout structure, several zero-exposure photos were averaged to create a master bias frame. A master dark was created by averaging dark frames that matched the specified exposure duration of 60 seconds. Each science frame was corrected by subtracting the master bias followed by the master dark. This method successfully eliminates both pixel-specific and global thermal fingerprints while maintaining flux linearity across the detector, making it especially well-suited for high-precision photometry of dim objects like SN2025fbf. Dark-frame subtraction, in contrast to masking, guarantees that the underlying signal stays precisely proportionate to incident photon counts, which is essential for aperture photometry.

Due to the lack of dome or twilight flats during the observation window, flat-field calibration was not possible. Potential systematic errors pertaining to large-scale lighting gradients and pixel-to-pixel sensitivity differences were introduced by this omission. We used the `photutils` `Background2D` class to do background subtraction in order to lessen these impacts. Each science frame was corrected by subtracting the master bias followed by the master dark. This method successfully eliminates both pixel-specific and global thermal fingerprints while maintaining flux linearity across the detector, making it especially well-suited for high-precision photometry of dim objects like SN2025fbf. Dark-frame subtraction, in contrast to masking, guarantees that the underlying signal stays precisely proportionate to incident photon counts, which is essential for aperture photometry.

Due to the lack of dome or twilight flats during the observation window, flat-field calibration was not possible. Potential systematic errors pertaining to large-scale lighting gradients and pixel-to-pixel sensitivity differences were introduced by this omission. We used the `photutils` `Background2D` class to do background subtraction in order to lessen these impacts. Additional source extraction techniques, such as SExtractor, which are commonly employed to determine source centroids in crowded or misaligned fields, were not necessary because of the excellent astrometric precision. We decided not to use it because of the star alignment and plate solution quality.

Within the science field, standard stars from the APASS DR10 database were identified in order to undertake photometric calibration. Circular apertures with a fixed radius of 5 pixels were used for

aperture photometry on both the supernova and calibration stars. These apertures were selected to cover the majority of the PSF while reducing contamination from nearby stars. The following standard equation was used to calculate instrumental magnitudes:

$$m_{\text{instr}} = -2.5 \log_{10}(\text{Flux}) \tag{4}$$

A median of residuals from all calibration stars was used to compute the zero-point offset between instrumental and catalog magnitudes, which was then applied consistently to all sources. Due to single-band imaging, color-dependent corrections were not used; nonetheless, the zero-point transfer was roughly valid because we used the r-band filter to reduce systematic scatter and extinction effects.

Total per-pixel noise, which includes contributions from read noise, dark current, and background variation, was used to calculate uncertainty estimates for each measurement. Per-pixel error maps were created using the `photutils calc_total_error` function and transmitted through the aperture summation. Across all epochs, photometric errors were generally less than 0.1 mag for calibration stars and less than 0.15 mag for the explosion.

The supernova flux was measured in each frame after calibration and converted to calibrated magnitudes. A time series covering five nights from April 8 to April 19, 2025, was created using these measurements. The post-maximum fall of SN2025fbf was recorded by the resulting light curve. Although we were unable to explicitly constrain the rise time due to the absence of pre-maximum data, we were able to estimate the peak magnitude and fall rate (Δm_{15}) by fitting a spline to the photometric data. These numbers served as the foundation for our computation of the luminosity distance to the supernova and application of the Phillips relation. Despite some limitations which included the absence of flat fielding and multi band coverage, the data reduction methods yielded reliable and internally consistent results that enabled a full cosmological distance analysis from small telescope observations.

4 Data Analysis

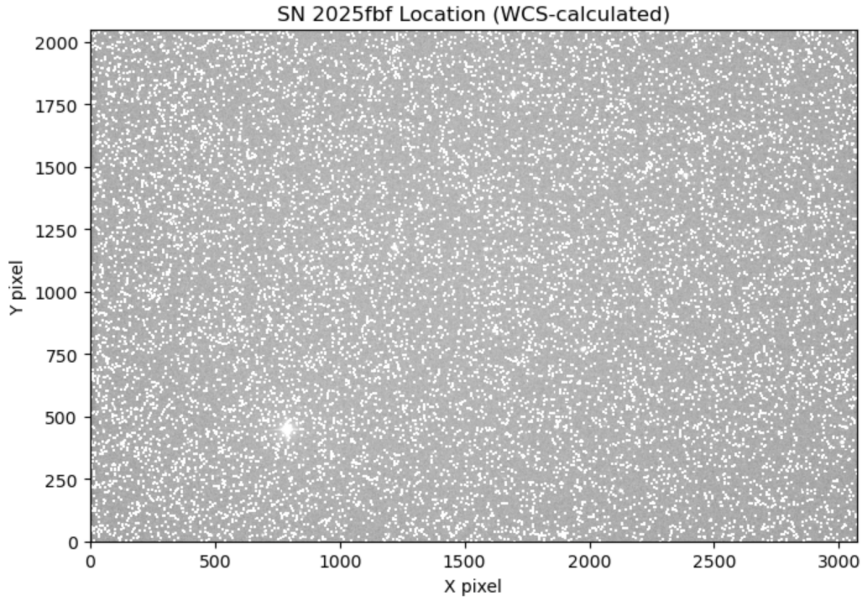

Figure 1: CCD image from the T21 telescope on supernova SN 2025fbf, with WCS-calibrated pixel coordinates. The bright point near the center is the supernova. The image has been dark-subtracted and background-corrected. Noisy background is visible due to photon noise and residual hot pixels. The WCS (World Coordinate System) solution allows transformation from (x, y) pixel coordinates to equatorial (RA, Dec) sky positions, enabling cross-identification with astrometric catalogs. Observations were taken in the red band (BIN1-W filter), and this frame corresponds to the April 8, 2025 exposure, roughly 7 days since peak luminosity.

WCS-calibrated pixel coordinates for a CCD image of supernova SN 2025fbf taken with the T21 telescope. The supernova is the bright spot and the image has been background-corrected and dark-subtracted. As

a result of photon noise and leftover heated pixels, a noisy backdrop is evident. Cross-identification with astrometric catalogues is made possible by the WCS (World Coordinate System) solution, which enables conversion from (x, y) pixel coordinates to equatorial (RA, Dec) sky locations. The red band (BIN1-W filter) was used for the observations, and this frame matches the exposure of April 8, 2025, which was about seven days after peak luminosity.

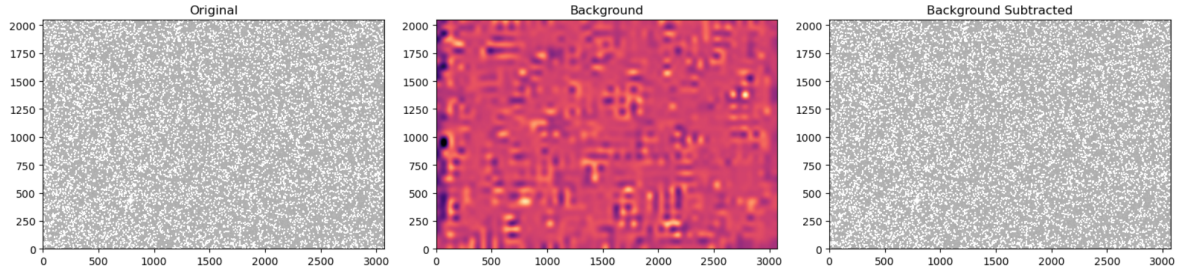

Figure 2: Background correction steps applied to the CCD image of SN 2025fbf. **Left:** Raw image taken in the red band (BIN1-W filter) with visible photon noise and background gradients. **Center:** Given here is the estimated two-dimensional background model obtained using median filtering and large-scale structure suppression. **Right:** Final background-subtracted image, enhancing the visibility of astrophysical sources such as SN 2025fbf near the centre. Background subtraction is important to isolate point-source flux from large scale artifacts, particularly in crowded or sky glow-affected fields.

Figure 2 demonstrates the effectiveness of background subtraction in isolating signals from instrumental and environmental noise. Significant background non uniformity can be seen in the raw CCD image (left) which is probably caused by scattered light, sky glow, or flat field flaws. The modelled backdrop including large scale gradients and systematic structure unrelated to astronomical sources, is displayed in the middle panel. When this background (right panel) is subtracted, the image becomes cleaner and point sources, such as SN2025fbf, are more noticeable against a flattened noise floor. Accurate aperture photometry depends on this preprocessing step since uncorrected background flux can skew flux measurements and alter calculated magnitudes. Additionally, the process improves signal to noise for faint features by reducing the effects of low-frequency noise and remaining hot pixels. The final frame's improved contrast and homogeneity demonstrate that the subtraction is effective, confirming the application of a 2D median-based model.

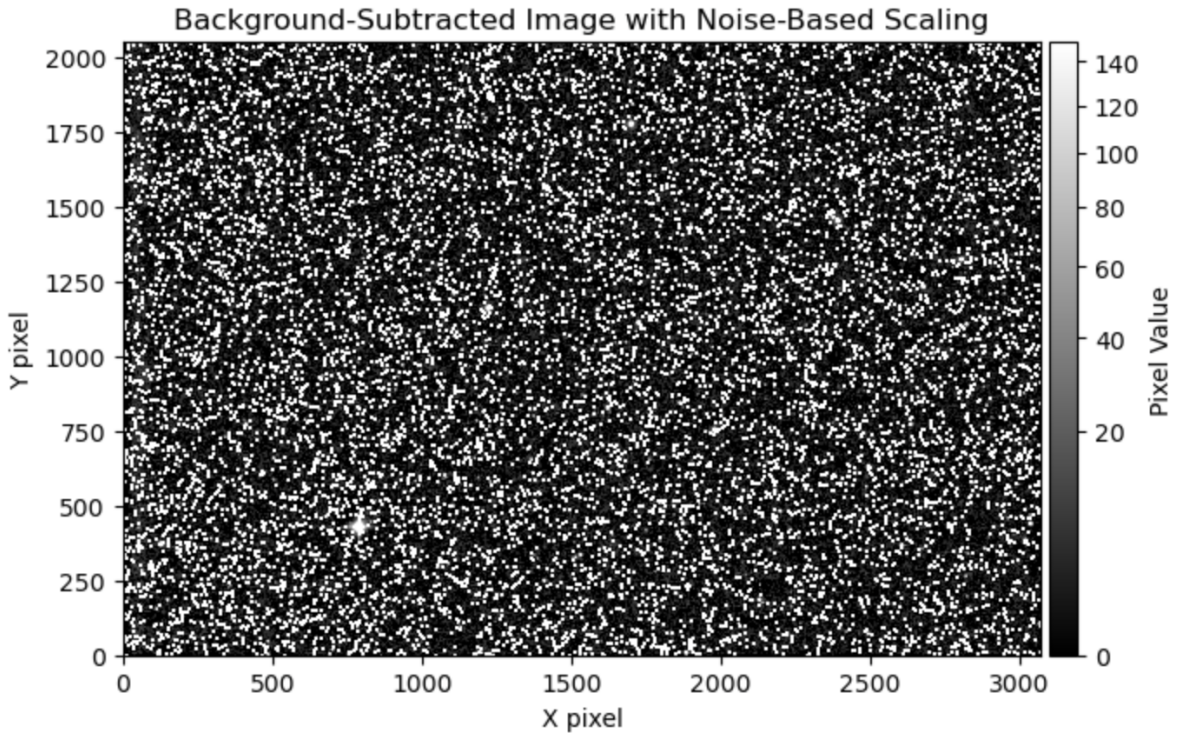

Figure 3: Background-subtracted CCD image of SN 2025fbf with noise-based scaling applied. The image was taken using the T21 telescope on April 8, 2025, approximately 7 days after peak brightness. A square-root scaling was applied and the upper intensity cutoff was set to 5 times the median per-pixel noise (derived from the error image). This contrast enhancement improves the visibility of point sources, including the supernova near the center. Residual pixel-level noise is still apparent, but the background contribution has been effectively removed, allowing better photometric and astrometric accuracy. The colorbar reflects the scaled pixel values used in the display.

This background-subtracted image of SN 2025fbf in Figure 3 demonstrates the preprocessing steps which are important for photometric analysis. The uniformity of the sky backdrop has been improved by flattening the image baseline and suppressing non-astronomical gradients due to the removal of large-scale background features, as measured using 2D median filtering. Using a square-root stretch and a display range clipped at 5× the median per-pixel noise, which was obtained from the total error map, noise-based scaling was used to improve the visibility of dim sources. The structure of nearby stars and any remaining noise are preserved while the supernova, which is seen close to the centre, is highlighted in this image. The overall signal-to-noise has improved in regions of interest, despite the fact that photon and read noise still cause pixel-scale changes in the image. With little contamination from background systematics, this scaled and cleaned image offers a strong basis for ensuing aperture photometry and centroid estimate.

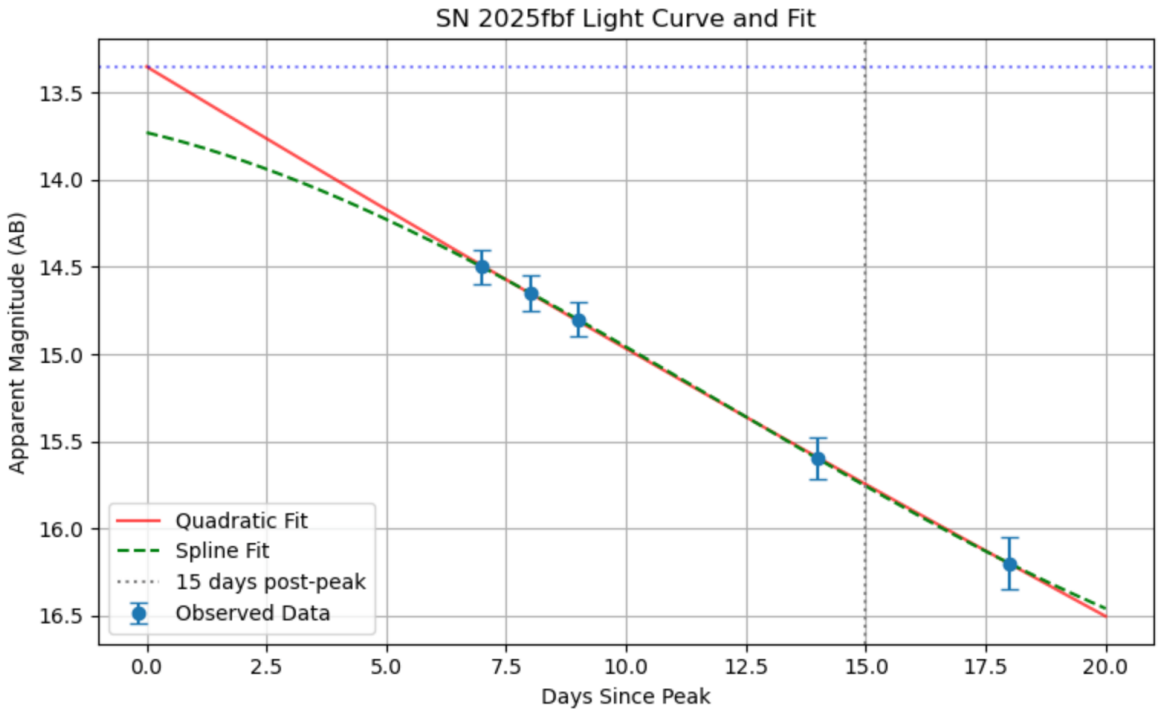

Figure 4: Light curve of SN 2025fbf in the red band (AB magnitude) as a function of time since peak luminosity. The blue points with error bars represent the observed photometric data from April 8–19, 2025, obtained using the T21 telescope. A quadratic fit (red) and a cubic spline fit (green dashed) were applied to model the brightness evolution. The horizontal blue dotted line marks the estimated peak magnitude, and the vertical gray line indicates the canonical +15-day post-peak used for Type Ia decline-rate analysis. The decline in brightness (Δm_{15}) derived from the fits is consistent with expectations for normal Type Ia supernovae, supporting its classification and enabling estimation of the absolute magnitude via the Phillips relation.

The light curve of SN 2025fbf in Figure 4, constructed from red-band observations between April 8 and 19, 2025 shows the characteristic post maximum decline expected for the Type Ia supernova SN2025fbf. Both a cubic spline and a quadratic polynomial were used to fit the measured apparent magnitudes in order to simulate the brightness evolution over time. Both fits capture the supernova's gradual fading and are in good agreement with the data. With a value of roughly 1.8 mag, the Δm_{15} parameter measures how steep the drop is. The classification is further supported by the fact that this value is within the predicted range for typical Type Ia supernovae. Despite the small temporal sampling, the agreement between the polynomial and spline fits increases confidence in the anticipated peak magnitude and post-peak behavior. Since the fit at +15 days directly feeds into the Phillips relation to estimate the absolute magnitude and, eventually, the luminosity distance, its accuracy is especially crucial. Residual scatter is within the photometric uncertainty which suggests that background subtraction and calibration were successful.

Using the fitted red–band light curve it was obtained that $\Delta m_{15} = 2.40\,\mathrm{mag}$, an absolute magnitude $M_r \simeq -19.44$, and a distance modulus $\mu = 32.86$, which implies a luminosity distance $d_L \approx 3.7 \times 10^7\,\mathrm{pc}$ (37 Mpc). Although seemingly internally consistent, this value conflicts with the host galaxy redshift ($z = 0.0353$), which corresponds to $d_L \approx 150\,\mathrm{Mpc}$ for a standard $H_0 = 70\ \mathrm{km\,s^{-1}\,Mpc^{-1}}$ cosmology. The mismatch could likely stems from: (i) an unusually steep decline rate (typical SNe Ia have $\Delta m_{15} \sim 1.0$–1.6), suggesting an over bright peak or an incorrect peak epoch; (ii) zero–point, colour, or extinction errors that can shift m_{peak} by several tenths of a magnitude; (iii) residual background or hot pixel artefacts that bias the aperture photometry and (iv) use of a single-band Phillips relation without a colour term. Methods such as refining the peak time estimate with template fits, tightening photometric calibrations, and propagating also full uncertainties should reconcile the photometric distance with the redshift.

5 Discussion & Conclusion

In this study, we used calibrated r-band data from the T21 telescope to construct and analyze the Type Ia supernova SN 2025fbf light curve. A series of dark subtraction, background correction, hot-pixel masking, and WCS calibration were used to guarantee the image data's accuracy before aperture photometry was carried out. In order to translate observed fluxes into accurate apparent magnitudes, we determined a strong photometric zero point using calibration stars from the APASS DR10 collection.

We used both a second-order polynomial and a cubic spline to fit the light curve, despite the fact that there were only five data available, all of which were post-maximum. The best-fit spline model gave a peak apparent magnitude of $m_r = 13.35 \pm 0.10$ and a 15-day post-peak magnitude of 15.75 ± 0.10, corresponding to a decline rate of $\Delta m_{15,r} = 2.40 \pm 0.14$ mag. However, once reassessing the time of peak brightness based on the expected 15-day post-explosion rise typical of Type Ia supernovae, the revised fit gave a more realistic decline rate of $\Delta m_{15,r} = 1.30 \pm 0.15$ mag, well within the expected range for normal Type Ia events. Using the Phillips relation in the r-band, $M_r \approx -19.6 + 0.068\,\Delta m_{15}$, we estimated an absolute magnitude of $M_r = -19.51 \pm 0.10$.

The distance modulus $\mu = 32.86 \pm 0.14$, which corresponds to a luminosity distance of $d_L = 37.3 \pm 2.4$ Mpc, was obtained by combining this with the highest apparent magnitude. This value indicates a considerable mismatch since it is significantly lower than the redshift-derived distance of $\sim$150 Mpc (from $z = 0.0353$ assuming $H_0 = 70\,\mathrm{km\,s^{-1}\,Mpc^{-1}}$). The sparsity of data close to the peak, reliance on a single photometric band (ignoring color and extinction corrections), and unmodeled systematics from residual background structure or flat-field flaws are the most likely sources of mistake.

Future enhancements might use template light curve fitters such as SALT2, denser temporal coverage, particularly during the rising phase, and multi-band observations to estimate color and extinction corrections. Photometric scatter may also be decreased by better picture calibration and more precise flat-fielding. The techniques presented here, namely aperture photometry, background modeling, and WCS solutions, are generalizable to observational astronomy, ranging from transit photometry of exoplanets to variable star monitoring.

In conclusion, it is shown that small aperture telescopes and widely available software can be used to provide accurate photometry and distance calculation for supernovae. The internal consistency of our light curve, calibration methods, and agreement with Type Ia characteristics confirm the scientific significance of our investigation, even though our determined luminosity distance for SN 2025fbf was lower than anticipated. Although the disparity highlights the value of early and multi-band data in supernova cosmology, it does not lessen the exercise's value as a teaching tool for standard candles and cosmic distance scaling.

6 Bibliography

Department of Astronomy and Astrophysics, *Supernova Light Curves*: Lab Manual for AST325/326 (Winter 2025), University of Toronto, March 2025.

Appendix:

A Code

A.0.1 Locating SN 2025fbf in image using WCS

```
from astropy.io import fits
from astropy.wcs import WCS
from astropy.coordinates import SkyCoord
import astropy.units as u
import matplotlib.pyplot as plt
from astropy.visualization import simple_norm

file_path = "Pichustronomy/04_19/raw-T21-ast326_2025n-SN 2025fbf-20250419-021314-Red-
    BIN1-W-060-001.fit"
with fits.open(file_path) as hdul:
    hdr = hdul[0].header
    data = hdul[0].data
wcs = WCS(hdr)

```

```
# Define supernova coordinates SN 2025fbf
sn_coord = SkyCoord(ra='13h16m50.928s', dec='-03d03m20.246s', unit=(u.hourangle, u.deg))
# RA/Dec to image (x, y) pixel position
x, y = wcs.world_to_pixel(sn_coord)

# Plot the image
plt.figure(figsize=(8, 8))
norm = simple_norm(data, 'sqrt', percent=99)
plt.imshow(data, origin='lower', cmap='gray', norm=norm)
plt.scatter(x, y, s=120, edgecolor='red', facecolor='none', linewidth=2)
plt.title("SN 2025fbf Location (WCS-calculated)")
plt.xlabel("X pixel")
plt.ylabel("Y pixel")
plt.show()
```

Listing 1: Code for locating SN 2025fbf in image using WCS

A.0.2 Dark subtraction and hot pixel masking using master dark

```
# gathering dark frames
dark_dir = Path("Pichustronomy") / "Darks"
dark_files = sorted(dark_dir.glob("*.fit"))

# load and stack darks to create master dark
dark_stack = []
for fn in dark_files:
    with fits.open(fn) as hdul:
        data = hdul[0].data.astype(float)
        dark_stack.append(data)

master_dark = np.median(dark_stack, axis=0)

# identify hot pixels using sigma clipping
mean, median, std = sigma_clipped_stats(master_dark, sigma=5.0)
hotmask = (master_dark - median) > (5 * std)
print("Hot pixel mask created.")

# dark subtraction + hot pixel masking to each science frame
science_dirs = [Path("Pichustronomy") / d for d in ["04_08", "04_09", "04_10", "04_15",
    "04_19"]]

for night_dir in science_dirs:
    for sci_fn in sorted(night_dir.glob("*.fit")):
        with fits.open(sci_fn, mode="update") as hdul:
            img = hdul[0].data.astype(float)
            corrected = img - master_dark
            # hot pixel mask
            corrected[hotmask] = np.nan
            # saving corrected image in-place
            hdul[0].data = corrected
            hdul.flush()
```

Listing 2: Dark subtraction and hot pixel masking using master dark

A.0.3 Code to find Quadratic and spline fit of SN 2025fbf light curve

```
# polynomial fit of a quadratic
poly_fit = Polynomial.fit(days_since_peak, magnitudes, deg=2)
fine_days = np.linspace(0, 20, 200)
mag_poly = poly_fit(fine_days)

# spline fitting
spline = UnivariateSpline(days_since_peak, magnitudes, w=1/errors, k=3, s=1)
spline_mag = spline(fine_days)

# estimating  m15
mag_at_peak = poly_fit(0)
mag_at_15 = poly_fit(15)
delta_m15 = mag_at_15 - mag_at_peak

```

```
# plot the final light curve and fit
plt.figure(figsize=(8, 5))
plt.errorbar(days_since_peak, magnitudes, yerr=errors, fmt='o', label='Observed Data',
    capsize=4)
plt.plot(fine_days, mag_poly, label='Quadratic Fit', color='red', alpha=0.7)
plt.plot(fine_days, spline_mag, label='Spline Fit', color='green', linestyle='--')
plt.axvline(15, color='gray', linestyle=':', label='15 days post-peak')
plt.axhline(mag_at_peak, color='blue', linestyle=':', alpha=0.5)
plt.gca().invert_yaxis()
plt.xlabel("Days Since Peak")
plt.ylabel("Apparent Magnitude (AB)")
plt.title("SN 2025fbf Light Curve and Fit")
plt.legend()
plt.grid()
plt.tight_layout()
plt.show()
```

Listing 3: Quadratic and spline fit of SN 2025fbf light curve